

Simple generic picture of toughness in solid polymer blends

Debashish Mukherji,^{1,*} Shubham Agarwal,^{2,†} Tiago Espinosa de Oliveira,^{3,†} Céline Ruscher,^{2,†} and Jörg Rottler^{1,4}

¹*Quantum Matter Institute, University of British Columbia, Vancouver BC V6T 1Z4, Canada*

²*Department of Mechanical Engineering, University of British Columbia, Vancouver BC V6T 1Z4, Canada*

³*Departamento de Farmacociências, Universidade Federal de Ciências da Saúde de Porto Alegre, Porto Alegre 90050-170, Brazil*

⁴*Department of Physics and Astronomy, University of British Columbia, Vancouver BC V6T 1Z1, Canada*

Toughness \mathcal{T} of a brittle polymeric solid can be enhanced by blending another compatible and ductile polymer. While this common wisdom is generally valid, a generic picture is lacking that connects the atomistic details to the macroscopic non-linear mechanics. Using all-atom and complementary generic simulations we show how a delicate balance between the side group contact density of the brittle polymers ρ_c and its dilution upon adding a second component controls \mathcal{T} . A broad range of systems follows a universal trend in \mathcal{T} with $d\rho_c/d\varepsilon$, where ε is the tensile strain. The simulation data is consistent with a simple model based on the parallel spring analogy.

Polymers are widely used in designing light weight, high performance organic materials [1–5] that find use in common household utensils to complex nano-materials [1, 2, 6–8]. Because of their wide applicability, these materials are often exposed to a range of environmental conditions, such as temperature [9–12], pressure [10, 13], and/or mechanical deformation [7, 9, 14–16]. Here, one important materials property is the ability to sustain large deformation [5, 16–19].

Most known commodity polymers, such as poly(methyl methacrylate) (PMMA) [15, 16], poly(lactic acid) (PLA) [5, 16], and polystyrene (PS) [20], are brittle in their glassy states, i.e., small strain-to-fracture ε_f and low yield stress $\sigma_y \simeq 0.1$ GPa due to the weak van der Waals (vdW) monomer-monomer interactions, the strength of which is about $k_B T$ at room temperature, where k_B is the Boltzmann constant [21]. On the other hand, σ_y of a polymer can be enhanced by about an order of magnitude when the monomer-monomer hydrogen bonds (H–bond), with an interaction strength of about $4k_B T$ [4], dominate the materials properties, such as in poly(acrylamide) (PAM), poly(acrylic acid) (PAA), and poly(vinyl alcohol) (PVA). These H–bonded systems, however, can either be brittle or ductile dependent on their respective (macro-)molecular architectures. Given the above discussion, mechanical response remains restricted in the single component polymeric systems and thus often limits their broad applications.

A simple route to tune the tensile toughness $\mathcal{T} = \int_0^\infty \sigma(\varepsilon) d\varepsilon$ of a brittle organic solid is by blending in another polymer with a relatively larger ductility and component-wise interactions. Here, σ and ε are the tensile stress and tensile strain, respectively. Experimentally relevant examples include, but are not limited to, PMMA-PLA [16, 22], PAA-PVA blends [18], and/or PMMA-PVA [23]. These systems are assumed to be fairly miscible, while abstaining to discuss the effects of immiscibility.

In general, \mathcal{T} of a blend varies monotonically between the two pure phases as a function of their relative mixing ratios [18]. However, a set of recent experiments on

PMMA-PLA blends have reported a non-monotonic variation in \mathcal{T} with concentration [16]. This behavior was attributed to the formation of “so called” co-continuous phase, with an estimated length scale on the order of several μm [16, 22]. However, a set of relatively much smaller scale all-atom simulations have found a similar trend in \mathcal{T} [24], suggesting that the formation of a co-continuous phase may not be a necessary criterion for the toughness enhancement in these materials.

Traditionally, extensive research has been conducted to understand the mechanics of polymeric materials, both from the experimental [5, 16, 18, 20] and the simulation [14, 15, 17, 24] communities. Here, however, most simulation studies usually deal with single component systems and also predominantly at the (mesoscopic) generic level, where all-atom details are drastically coarse-grained [21]. While such models are extremely useful in dealing with generic polymer properties, they often (in their pristine form) lack the atomic-level details that play a key role in materials properties, unless of course the generic model is specifically tuned to reproduce certain properties of interest. In particular, when dealing with polymer blends having very specific macromolecular structures and interactions [16, 18, 24], special attention should be paid. Therefore, a better understanding of the monomer-level (atomistic) interaction is needed to achieve a predictive mechanical response of the polymer blends, which to the best of our knowledge is lacking.

In this work, we investigate the mechanics of commodity organic solids with the goals to: (1) understand the effect of blending on the mechanics of brittle systems, (2) show how the monomer (atomistic) structures play a key role in dictating the materials properties, (3) connect the atomistic interaction details to the macroscopic non-linear mechanics, and (4) propose how the behavior of many different chemically specific polymeric materials can be understood within one universal framework. To achieve the above goals, we combine all-atom and complementary generic molecular dynamics simulations with a simple parallel spring model.

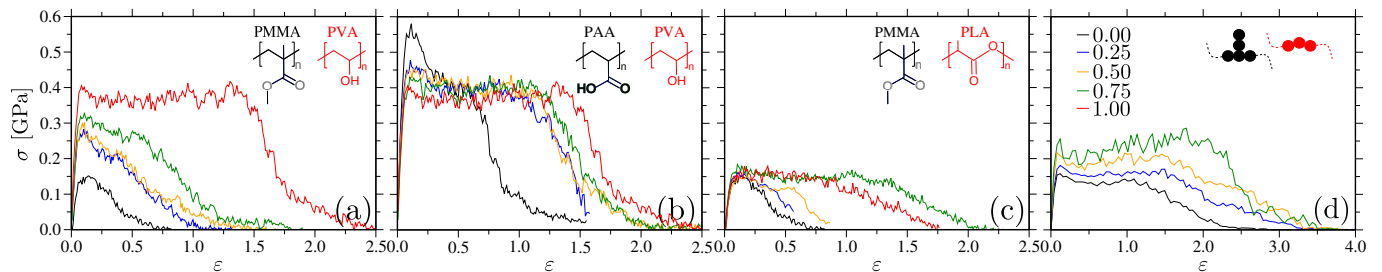


FIG. 1: Stress σ as a function of strain ϵ for three different atomistic blends, namely poly(methyl methacrylate) (PMMA) and poly(venyl alcohol) (PVA) (panel a), poly(acitic acid) (PAA) and PVA (panel b), PMMA and poly(lactic acid) (PLA) (panel c), and the generic model (panel d). The data is shown for five different PVA and PLA and four (generic) linear chain monomer mole fractions x_i . Here, $x_i = 0.0$ corresponds to the pure brittle phase. The corresponding monomer structures are shown in the insets. σ for the generic model is converted using a factor $p_o = 40$ MPa [21]. Note that the data for PMMA-PLA blends are taken from Ref. [24].

For the all-atom simulations, we have chosen both vdW and H-bonded (experimentally relevant) commodity polymers (i.e., PMMA, PAM, PAA, PLA, and PVA) and polymer blends (i.e., PMMA-PVA, PAA-PVA, and PMMA-PLA). Note that we have performed the simulations for all systems in this work, aside from the PMMA-PLA trajectories which were obtained earlier [24] and reanalyzed here. The monomer mole fractions are varied between $0.0 \leq x_i \leq 1.0$ in steps of 0.25. In this study, $x_i = 0.0$ always corresponds to the pure phase of brittle polymer (BP) and the pure second polymer (SP) at $x_i = 1.0$. The OPLS-AA parameters are used for PAA, PLA, and PVA [25], while the modified force-field parameters are used for PAM [26] and PMMA [27]. The chain length $N_\ell = 30$ monomers is chosen for all systems except PAM, where $N_\ell = 32$. The simulations are performed using the GROMACS molecular dynamics package [28]. More system specific details are shown in the Supplementary Section S1A [29].

The well known bead-spring polymer model is used for the generic simulations [21]. Note that the default bead-spring model is highly ductile [14]. Therefore, inspired by the all-atom BP architectures, we have parameterized a brush-like polymer with short (stiff) side groups of the dimers, blended with the (ductile) linear chains. The monomer-monomer interactions are tuned to weakly mimic the atomistic PMMA-PVA blends. The backbone chain length is taken as $N_\ell = 30$. The generic simulations are performed using the LAMMPS package [30]. A detailed discussion of the generic model is described in the Supplementary Section S1B [29]. The numbers that are representative of hydrocarbons are: the units of length $d = 0.5$ nm, energy $\epsilon = 30$ meV, time $t_o = 3$ ps, and pressure $p_o = 40$ MPa [21]. Note that for simplicity of presentation, we have converted all generic units into the real units.

In Figs. 1(a-c) we show stress-strain behavior of three different all-atom blends under uniaxial tensile deformation. As expected, blending in SPs drive the BP-

based systems to a greater ductility, especially because the pure SPs are relatively more ductile than BPs. Ideally one can argue, if SPs have their glass transition temperatures T_g much smaller than BP (thus remain in their rubbery phases), the ductility or \mathcal{T} may increase via rubber plasticity. In our case, however, all polymers have $T_g \simeq 355 - 390$ K (as measured in the experiments) [16, 31], while the simulations have reported $T_g \simeq 400$ K [24, 32]. In this context, our simulations are performed at $T = 300$ K and thus $T_g - T$ are such that the individual components of a blend remain deep in their respective glass phases [31, 32]. This readily excludes any explanation purely based on T_g , and it becomes apparent that a nanoscopic picture is needed to better understand the nonlinear mechanics of the multi-component polymeric materials.

A comparative analysis of the monomer structures of BP and SP reveals that one major difference between these two sets is the presence of bulky side groups in BPs (see PAA and PMMA structures in Fig. 1), while SPs are smooth (see PVA and PLA structures in Fig. 1). In this context, it is known that the side groups of BPs are rather stiff and thus form extremely rugged (instantaneous) structural corrugation along the chain contour. Corrugation (or more generally speaking, the breaking of translational Galilean invariance) is a necessary “ingredient” to exert the shear forces upon deformation. Note also that the side groups can flip-flop normal to the chain contour in the polymer melt, while these structural fluctuations are frozen in the glassy state. In this context, it has been shown previously that the presence of stiff side chains may serve as a necessary criterion to control the brittleness in a solid PMMA [15].

Within the picture discussed above, the side groups of two or more neighboring chains can interlock, shown by the schematic in Fig. 2(a). Here, the interlocking can be dictated by either vdW or H-bond interactions. When a pure BP glass is deformed, the rigid side chain contacts break via relative motion of the chains and thus the slid-

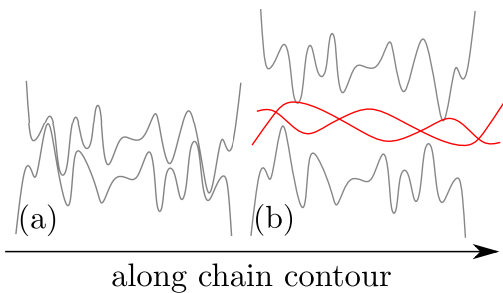


FIG. 2: Schematic representations of the direct contacts between the brittle polymers (BP) before (panel a) and after including the second polymer (SP) (panel b). For the simplicity of presentation, the one-dimensional projection of the effective roughness (or the effective free energy landscape) of the molecules along the chain contours is shown. The grey and red lines represent (rugged) BP and (smooth) SP molecules, respectively.

ing molecules overcome the effective free energy barriers. Such broken contacts initiate cavitation at around the yield strain, i.e., $\varepsilon_y \simeq 0.1 - 0.2$, see Fig. 1. Beyond ε_y , the systems go into the flow regime with growing voids, leading to their coalescence and ultimate fracture. The stronger the side chain contacts, the larger the σ_y values. In this context, we find $\sigma_y^{\text{PMMA}} < \sigma_y^{\text{PAA}} < \sigma_y^{\text{PAM}}$, see the supplementary Fig. S8 [29]. This is expected because two PMMA side chains interact via weak vdW interaction, while two PAA and two PAM can form 0.84 and 1.52 H-bonds per monomer, respectively.

When the SP molecules are added, they lubricate and also dilute the density of side chain contacts ρ_c between the neighboring BPs, see the schematic in Fig. 2(b). This microscopic molecular arrangement increases ε_f and also hinders the growing voids via rearrangements of SPs. Here, the extent of molecular ruggedness that a molecule feels, while moving in the homogeneous bulk, is directly related to x_i and thus has a direct implication on the polymer motion. The mean-square-displacement $C(t)$ data, shown in the Supplementary Figs. S2 & S3, provide evidence that the molecular diffusion D increases with increasing x_i . Within the linear response, the different damping contributions are linearly additive and thus the effective damping $\gamma \propto 1/D$. Furthermore, following $C(t)$ in the Supplementary Figs. S2 & S3, it becomes apparent that the atomic level ruggedness (or corrugation) reduces with increasing x_i . In the glassy state, we also expect the relative ruggedness across different samples to remain the same. The statement above does not aim to make a direct quantitative comparison between the melt and the glassy states, rather only a qualitative discussion without attempting to discuss the time-temperature superposition.

We note in passing that the systems investigated in this study have larger ductility than the experimentally reported values [5, 16, 18, 20]. This is particularly be-

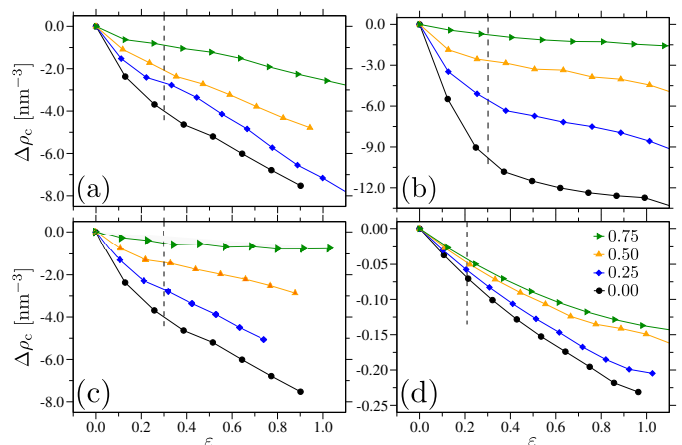


FIG. 3: Density of side chain contacts $\Delta\rho_c = \rho_c(\varepsilon) - \rho_c(0)$ as a function of strain ε between the neighboring monomers of the brittle polymers in the blends of poly(methyl methacrylate) (PMMA) and poly(vinyl alcohol) (PVA) (panel a), poly(acrylic acid) (PAA) and PVA (panel b), PMMA and poly(lactic acid) (PLA) (panel c) and the generic model (panel d). For better visibility of the relative variation in the data, we have shifted all curves with respect to $\rho_c(0)$ of the unstrained system, i.e., at $\varepsilon = 0$. In the generic model, $d\rho_c/d\varepsilon$ is scaled using the unit conversion $d = 0.5 \text{ nm}$ [21]. Data for PLA-PMMA blends is derived from our earlier simulation trajectories in Ref. [24]. The vertical dashed lines show the ε values at the yield points, see Fig. 1.

cause the quenching rates (i.e., from melt-to-glass) in the simulations are usually several orders of magnitude faster than the corresponding experiments and thus lead to poorer annealed samples [33]. Such samples usually have residual σ distributions that are rather broad, while well-annealed samples have narrow distribution in σ and thus all sites fail almost at once upon loading, leading to a smaller ε_f in experiments in comparison to the standard simulations. Here, however, it is important to note that our simulation samples are all prepared using an identical protocol and considering that this study aims at the relative trends, we believe that the data sets presented in Fig. 1 give a reasonable relative picture.

If the observation discussed above is generic, the trends in Figs. 1(a-c) should also be visible in a chemically independent model by only incorporating the monomer structures. Therefore, we have also conducted one set of generic simulations. Here, a BP consists of a bottle brush-like polymer with short, stiff side groups, while a SP is represented by a standard (fully flexible) linear bead-spring chain [21]. In Fig. 1(d) the generic data is presented. It can be appreciated that the trend observed in Fig. 1(a-c) is also reproduced by the generic model.

So far we have only presented a qualitative picture of the results. It will, however, be useful to draw more quantitative comparisons between the side chain contact density $\rho_c(\varepsilon)$ and \mathcal{T} . Here, $\rho_c(\varepsilon) = N_c(\varepsilon)/v(\varepsilon)$, with $N_c(\varepsilon)$ and $v(\varepsilon)$ being the number of side chain contacts and the

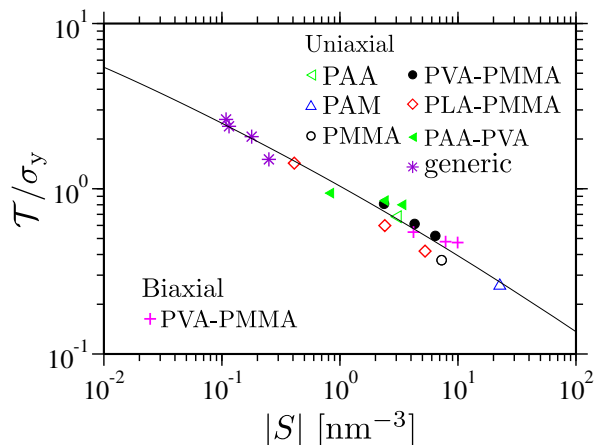


FIG. 4: A master curve relating the normalized toughness \mathcal{T}/σ_y with the change in side chain contact density ρ_c upon deformation, as quantified by the slope $S = d\rho_c(\varepsilon)/d\varepsilon$. The data is normalized with respect to the yield stress σ_y , calculated from Fig. 1. The line is a fit to the data using Eq. 2. While most data sets are shown for uniaxially deformed samples, we also present one case study in which a set of PMMA-PVA blends is biaxially deformed.

instantaneous system volume, respectively. In the all-atom simulations, $N_c(\varepsilon)$ is calculated when the center-of-masses of two neighboring (inter-molecular) side chains are within a minimum distance $r_{\min} \leq 0.65$ nm, i.e., the first peak of the radial distribution function [32, 34]. In the generic model, $r_{\min} \leq 1.5 \sigma$ [35].

In Fig. 3 we show $\rho_c(\varepsilon)$ for the all-atom and the generic models. It can be appreciated that: (a) ρ_c decreases with increasing ε , which is expected because the tensile deformation breaks the side chain contacts between BPs that lead to the ultimate fracture of the samples. (b) Increasing x_i generally dilutes $\rho_c(\varepsilon)$ and thus leads to the weaker decay rates for $\varepsilon > \varepsilon_y$ (shown by the vertical dashed lines in Fig. 3).

The individual data sets in Fig. 3 show two different $d\rho_c/d\varepsilon$ regions. The first is a relatively rapid decay for $\varepsilon_y < 0.2$ (in all-atom) and $\varepsilon_y < 0.1$ (in generic), where the $d\rho_c(\varepsilon)/d\varepsilon$ behavior is dominated by the initial disruption between the side groups, see Fig. 1. The second linear decay beyond ε_y occurs when the individual systems reach the flow (stationary) regime, where the voids grow and also SPs rearrange to control \mathcal{T} . We calculate the slopes $S = d\rho_c(\varepsilon)/d\varepsilon$ in the stationary flow regimes, where the behavior is reasonably well described by the simple linear form $\rho_c(\varepsilon) = \rho_o + S\varepsilon$.

Fig. 4 shows the variation of toughness-to-strength ratio \mathcal{T}/σ_y with S . It can be appreciated that a broad range of chemical specific systems and the generic model data fall onto one empirical master curve. Here, most data sets are obtained for uniaxial loading, where the mechanics is dominated by the shear force exerted by the sliding molecules. However, the data for the biaxial

loading, where the cavitation is enhanced (see the Supplementary Figs. S6 & S7), also support the same empirical behavior.

While the data sets in Fig. 4 show a correlation across several samples, it is important to investigate if this behavior can be understood within a model by incorporating some microscopic descriptions, which is achieved using a simple (mechanical) model. This is inspired by the parallel spring model analogy [36]. The model specific details are described in the Supplementary section S2 [29], here we only sketch the important ingredients. Within this model, an organic solid is modeled as a three-dimensional network of springs in parallel, where one side chain interlocking represents one spring contact with an effective spring constant k_i . Force F and local displacement δ then follows $F(\delta) = \sum_{i=1}^{N_c} k_i \delta$. If we consider that the all contacts contribute equally to the loading, i.e., $k_i \simeq k$, we get $F(\delta) = kN_c(\delta)\delta$. Under the affine assumption, the local (microscopic) displacement δ relates to the macroscopic displacement via $\delta = c\varepsilon L_o$. Here L_o is the unstrained box dimension and c is a (small) dimensionless constant. This assumes that each contact carry the same load and $\delta \ll \varepsilon L_o$, i.e., $c \ll 1$. Following σ from F (see the Supplementary section S2 [29]), we obtain

$$\frac{\mathcal{T}}{\sigma_y} = \frac{1}{\sigma_y} \int_0^{\varepsilon_f} \sigma(\varepsilon) d\varepsilon = \frac{ckL_o^2}{\sigma_y} \int_0^{\varepsilon_f} \rho_c(\varepsilon) \varepsilon (1 + \varepsilon) d\varepsilon. \quad (1)$$

Eq. 1 leads to an empirical solution,

$$S \simeq \frac{\left[\frac{\mathcal{T}}{\sigma_y} - \frac{ckL_o^2 \rho_o}{\sigma_y} \left\{ \frac{1}{2} \left(\frac{\mathcal{T}}{\sigma_y} \right)^2 + \frac{1}{3} \left(\frac{\mathcal{T}}{\sigma_y} \right)^3 \right\} \right]}{\frac{ckL_o^2}{\sigma_y} \left[\frac{1}{3} \left(\frac{\mathcal{T}}{\sigma_y} \right)^3 + \frac{1}{4} \left(\frac{\mathcal{T}}{\sigma_y} \right)^4 \right]}. \quad (2)$$

Eq. 2 is plotted as the solid line in Fig. 4, with $ckL_o^2 \rho_o / \sigma_y \simeq 0.01$. Note that the factor k/σ_y remains constant for a given sample. It can be appreciated that Eq. 2 follows a reasonable agreement with the simulation data in Fig. 4. This further reinforces a picture directing at a possible route towards the tunability in \mathcal{T}/σ_y and its links to the atomic level details.

It will certainly require more detailed experiments to validate our scenario. One plausible path might be to follow the protocol presented in an earlier study of one of us [37], where a proton nuclear magnetic resonance (NMR) setup was used to obtain the local side chain organizations between the neighboring non-bonded monomers. Here, we expect that the on-the-fly NMR measurements (at different ε) might give direct information about ρ_c and thus can lead to a better understanding of the underlying atomistic picture in these commodity organic solids.

In conclusion, we have performed large scale molecular dynamics simulations to study the mechanics of solid commodity polymer blends. We show how a delicate balance between the (macromolecular) side chain organizations, resultant corrugation along the chain contour, and

their interlocking controls the toughness \mathcal{T} of a polymeric material. Our study establishes a relationship between the microscopic interactions and the macroscopic nonlinear mechanics, which follows a universal empirical relationship across a wide range of polymeric systems. To better understand this behavior, we have also formulated a simple model based on the *springs in parallel* analogy. The simplified picture presented here may serve as a guiding tool for the development of advanced functional materials with tunable and predictive mechanical properties.

D.M. thanks Carlos Marques and Kurt Kremer for stimulating discussions. This research was undertaken thanks, in part, to the Canada First Research Excellence Fund (CFREF), Quantum Materials and Future Technologies Program. D.M. further thanks ARC Sockeye facility of the University of British Columbia where the simulations are performed.

* debashish.mukherji@ubc.ca

† Contributed equally to this work and the names are written alphabetically

- [1] M. A. Cohen-Stuart, W. T. S. Huck, J. Genzer, M. Müller, C. Ober, M. Stamm, G. B. Sukhorukov, I. Szleifer, V. V. Tsukruk, M. Urban, F. Winnik, S. Zauscher, I. Luzinov, and S. Minko *Nature Materials*, vol. 9, p. 101, 2010.
- [2] G. Kim, D. Lee, A. Shanker, L. Shao, M. S. Kwon, Gidley, J. Kim, and K. P. Pipe *Nature Materials*, vol. 14, pp. 295–300, 2015.
- [3] M. Müller *Progress in Polymer Science*, vol. 101, p. 101198, 2020.
- [4] D. Mukherji, C. M. Marques, and K. Kremer *Annual Reviews of Condensed Matter Physics*, vol. 11, pp. 271–299, 2020.
- [5] X. Zhao, H. Hu, X. Wang, X. Yu, W. Zhou, and S. Peng *RSC Adv.*, vol. 10, pp. 13316–13368, 2020.
- [6] W. Shi, Z. Shuai, and D. Wang *Advanced Functional Materials*, vol. 27, p. 1702847, 2017.
- [7] K. S. Toohey, N. R. Sottos, J. A. Lewis, J. S. Moore, and S. R. White *Nature Materials*, vol. 6, pp. 581–585, 2007.
- [8] M. Sharifi, C. W. Jang, C. F. Abrams, and G. R. Palmese *Journal of Materials Chemistry A*, vol. 2, pp. 16071–16082, 2014.
- [9] R. S. Hoy and M. O. Robbins *Journal of Polymer Science Part B: Polymer Physics*, vol. 44, no. 24, pp. 3487–3500, 2006.
- [10] V. A. Harmandaris, J. Floudas, and K. Kremer *Macromolecules*, vol. 44, no. 2, pp. 393–402, 2011.
- [11] W. Liu and W.-H. Zhai *Journal of Research Updates in Polymer Science*, vol. 4, pp. 139–148, 2015.
- [12] J. Wu and D. Mukherji *Computational Materials Science*, vol. 211, p. 111539, 2022.
- [13] W.-P. Hsieh, M. D. Losego, P. V. Braun, S. Shenogin, P. Keblinski, and D. G. Cahill *Physical Review B*, vol. 83, p. 174205, 2011.
- [14] J. Rottler and M. O. Robbins *Phys. Rev. E*, vol. 68, p. 011507, Jul 2003.
- [15] K. Fujimoto, Z. Tang, W. Shinoda, and S. Okazaki *Polymer*, vol. 178, p. 121570, 2019.
- [16] X. Hou, S. Chen, J. J. Koh, J. Kong, Y.-W. Zhang, J. C. C. Yeo, H. Chen, and C. He *ACS Macro Letters*, vol. 10, no. 4, pp. 406–411, 2021.
- [17] T. W. Rosch, J. K. Brennan, S. Izvekov, and J. W. Andzelm *Phys. Rev. E*, vol. 87, p. 042606, Apr 2013.
- [18] Q. Huang, C. Wan, M. Loveridge, and R. Bhagat *ACS Applied Energy Materials*, vol. 1, no. 12, pp. 6890–6898, 2018.
- [19] M. Huang and C. Abrams *Macromolecular Theory and Simulations*, vol. 28, p. 1900030, aug 2019.
- [20] P. Antich, A. Vázquez, I. Mondragon, and C. Bernal *Composites Part A: Applied Science and Manufacturing*, vol. 37, no. 1, pp. 139–150, 2006.
- [21] K. Kremer and G. S. Grest *The Journal of Chemical Physics*, vol. 92, no. 8, pp. 5057–5086, 1990.
- [22] K.-P. Le, R. Lehman, J. Remmert, K. Vanness, P. M. L. Ward, and J. D. Idol *Journal of Biomaterials Science, Polymer Edition*, vol. 17, no. 1-2, pp. 121–137, 2006.
- [23] A. Mohammed Kadim, A. Dheyaa Abdulkareem, A. Jawad Kadhim alrubaie, and K. Haneen Abass *Materials Today: Proceedings*, 2021.
- [24] D. Mukherji, T. E. de Oliveira, C. Ruscher, and J. Rottler *Phys. Rev. Materials*, vol. 6, p. 025606, Feb 2022.
- [25] W. L. Jorgensen, D. S. Maxwell, and J. Tirado-Rives *Journal of the American Chemical Society*, vol. 118, pp. 11225–11236, 1996.
- [26] T. E. de Oliveira, D. Mukherji, K. Kremer, and P. A. Netz *Journal of Chemical Physics*, vol. 146, p. 034904, 2017.
- [27] D. Mukherji, C. M. Marques, T. Stühn, and K. Kremer *Nature Communications*, vol. 8, p. 1374, 2017.
- [28] S. Pronk, S. Pall, R. Schulz, P. Larsson, P. Bjelkmar, R. Apostolov, M. R. Shirts, J. C. Smith, P. M. Kasson, D. van der Spoel, B. Hess, and E. Lindahl *Bioinformatics*, vol. 29, pp. 845–854, 2013.
- [29] “Electronic supplementary material. document number to be included by the editor.”
- [30] S. Plimpton *Journal of computational physics*, vol. 117, no. 1, pp. 1–19, 1995.
- [31] J. Brandrup, E. H. Immergut, and E. A. Grulke, “Polymer handbook, 2 volumes set, 4th edition,” 2003.
- [32] C. Ruscher, J. Rottler, C. E. Boott, M. J. MacLachlan, and D. Mukherji *Physical Review Materials*, vol. 3, p. 125604, 2019.
- [33] Quenching rates in simulations are usually significantly higher than the experiments due to the obvious computational limitations, especially when dealing with the all-atom trajectories of reasonably big system sizes. Of course, one can use particle swapping protocols to better anneal a system, which is, however, beyond the scope of our work.
- [34] L. Pigard, D. Mukherji, J. Rottler, and M. Müller *Macromolecules*, vol. 54, no. 23, pp. 10969–10983, 2021.
- [35] D. Mukherji and C. F. Abrams *Phys. Rev. E*, vol. 79, p. 061802, Jun 2009.
- [36] R. C. Picu *Soft Matter*, vol. 7, pp. 6768–6785, 2011.
- [37] D. Mukherji, M. Wagner, M. D. Watson, S. Winzen, T. E. de Oliveira, C. M. Marques, and K. Kremer *Soft Matter*, vol. 12, pp. 7995–8003, 2016.